Pharmaceutical Sciences and Drug Design
ISSN: 3062-4428
2026, Volume 6, Issue 1, Page No: 106-118

Available online at: www.galaxypub.co/page/journals

Galaxy Publication

Nitroreductase-Activated Nitrofurantoin Encapsulated in Cubosomes for Enhanced Breast Cancer Treatment

Fatima Zahra Amrani[1]*, Youssef Benali[1]

[1]Department of Pharmaceutical Chemistry and Drug Design, Faculty of Medicine and Pharmacy, Mohammed V University, Rabat, Morocco.

***E-mail** ✉ fatima.amrani@gmail.com

Received: 15 Nobvember 2025; **Revised:** 19 February 2026; **Accepted:** 26 February 2026

ABSTRACT

Nitrofurantoin (NITRO), a time-honored antibiotic prescribed for urinary tract infections, relies on nitroreductases for its activation. This mode of action has spurred its evaluation for drug repurposing aimed at controlling and managing breast cancer, a malignancy that expresses a nitroreductase gene. NITRO-loaded cubosomes were prepared by hot homogenization using a 23 full-factorial design. The variables examined consisted of the drug-to-oily phase proportion (1:10 and 2:10), the oily-to-aqueous phase proportion (1:10 and 1:5), and the Glyceryl mono-oleate (GMO)-to-Poloxamer 407 (PX407) proportion (0.25:1 and 0.5:1). Eight distinct formulations were planned and appraised based on particle size, zeta potential, polydispersity index, and entrapment efficiency percentage. Formulation S6 (configured with 1:10 drug: oily phase, 1:5 oily: aqueous phase, and 0.5:1 GMO: PX407), exhibiting a particle size of 45.5 ± 1.1 nm alongside an entrapment efficiency of 98.6% ± 1.8%, achieved the highest desirability score and was singled out for deeper evaluation. TEM examined its morphology. The activation of NITRO delivered from S6, as measured by intracellular viability of MCF-7 breast cancer cells, was assessed using an MTT assay. Data demonstrated that S6 yielded the lowest IC50 (83.99 ± 0.15 µg g/mL), compared with Free NITRO (174.54 ± 1.36 µg g/mL), indicating superior potency relative to the free drug. Nitrofurantoin cubosomes are viable prospects for repurposing in breast cancer therapy, contingent on additional stability assessments and in vivo studies.

Keywords: Nitro reductase, Glyceryl monooleate, Poloxamer 407, MTT assay, Factorial design

How to Cite This Article: Amrani FZ, Benali Y. Nitroreductase-Activated Nitrofurantoin Encapsulated in Cubosomes for Enhanced Breast Cancer Treatment. Pharm Sci Drug Des. 2026;6(1):106-18. https://doi.org/10.51847/OJK9SriAAJ

Introduction

Malignant disease, a complex and multidimensional disorder, involves uncontrolled cell division and ongoing genomic alterations that give rise to neoplastic traits in otherwise healthy cells [1, 2]. The core aim of any oncological intervention is to curb tumor expansion and metastatic spread, while averting relapse following clearance, ultimately lengthening the patient's lifespan [3]. Standard cancer treatment strategies—surgery, chemotherapy, and radiotherapy—carry inherent drawbacks, such as therapeutic resistance, profound toxicities, and an inability to target diseased tissue selectively [4]. As a result, these modalities often fall short of meeting patient expectations, creating a pressing need for fresh investigations to identify groundbreaking remedies [5].

Data from the World Health Organization indicate that roughly 2.3 million women received a breast cancer diagnosis in 2020, with 0.5 million succumbing to the disease each year [6, 7]. Radiotherapy is a widely used intervention [8] that is supplemented by a range of traditional chemotherapeutic agents [9]. The incorporation of nanoscale carriers has been established in oncological practice [10]. Such platforms include liposomes, polymeric nanoparticles, polymeric micelles, dendrimers [11], magnetic nanoparticles [12], and pH-responsive nano-vehicles [13]. Photodynamic therapy has likewise emerged as a potent anticancer modality [14]. This approach uses laser irradiation, which is both precise and well-tolerated by patients. Photodynamic therapy has also advanced the deployment of femtosecond laser technology for cancer care [15].

The concept of 'drug repositioning' entails deploying an existing pharmaceutical for a clinical indication beyond its original approval. This approach has attracted growing interest as it serves as an alternative to synthesizing entirely new drugs. One major benefit of repositioning is the wealth of pre-existing information available to researchers, which either eliminates or substantially reduces the need for studies assessing drug pharmacokinetics and toxicological profiles [16].

Nitrofurantoin (NITRO) belongs to the nitrofuran class, specifically a hydantoin-derived compound (1-[(E)-(5-nitrofuran-2-yl) methyl ideneamino] imidazolidine-2,4-dione), and is prescribed for the prevention and management of urinary tract infections. The agent works by disrupting bacterial DNA synthesis. Its nitro functional group is reduced by bacterial flavoenzymes (nitroreductases) [17], yielding reactive intermediates that subsequently form hydroxyl radicals. These radical entities interact with DNA, blocking nucleic acid production and causing both single- and double-strand DNA fragmentation [18, 19].

More recent findings, however, have revealed that nitrofurantoin may also exhibit cytotoxicity toward tumor cells expressing nitroreductase [5]. Laboratory-based investigations have shown that nitrofurantoin can suppress the proliferation of multiple cancer cell types, including those originating from the colon, prostate, and breast [20].

Consistent with this, nitro-containing antimicrobial agents that undergo enzymatic bioreduction of the nitro moiety produce metabolites that interfere with biomolecules critical for cell survival. Hence, such compounds possess anticancer potential against solid malignancies harboring oxygen-deprived zones [21]. The targeted cytotoxic effect of nitrofurantoin in hypoxic regions of solid tumors [22] is attributed to its conversion to a pharmacologically active form under low-oxygen conditions.

According to the Biopharmaceutics Classification System, nitrofurantoin is classified as class IV, indicating inadequate solubility and limited permeability [23]. Consequently, boosting its bioavailability requires a carrier platform that addresses both poor aqueous solubility and restricted permeability.

The field of nanotechnology has left a profound mark on cancer care by improving the performance of drug-delivery systems. Nanoparticles (NPs) offer multiple benefits, including refined pharmacokinetics, selective homing to neoplastic tissue, reduced toxicity, and the ability to overcome drug resistance [24]. Engineered to reflect tumor-specific traits, these NPs target malignant cells and deliver their payload to induce cellular death. They further aid in conveying poorly soluble compounds into systemic circulation, extending half-life in the body, and safeguarding healthy tissues from harm, thus diminishing the noxious side effects of oncological treatment [25]. For instance, nanoscale materials such as gold, silver, and copper exhibit extraordinary properties that make them highly suitable for immunosensor construction, and their use in cancer diagnostics has yielded outstanding results [26].

Lipid-based nanoparticles are instrumental in improving the solubility and permeability of therapeutic agents. Cubosomes represent a subtype of these lipid-centered nanoparticles [27]. These structures are Liquid Crystals (LCNs) that are widely recognized and utilized as drug carriers in conditions such as cancer [28]. A distinguishing strength of cubosomes is their ability to modulate membrane curvatures independently of particle diameter over considerable length scales. As a result, they support drug targeting, extended circulatory half-life, and sustained release kinetics [28]. Cubosomes are self-organized nanoparticulate systems derived from bulk bi-continuous cubic-phase lipids and stabilized using Pluronic. Their formulation can involve amphiphilic lipids, such as glyceryl monooleate (GMO), which spontaneously self-assemble in aqueous media to form cubosomes [29]. Phytantriol may serve as an alternative to GMOs, especially within cosmetic preparations [30]. The bi-continuous phase adopts a honeycomb-inspired, three-dimensional network. They contain cavern-like voids, enabling efficient encapsulation of therapeutic payloads [31-33]. The fabrication of cubosomes may follow a top-down [34] or a bottom-up [35] strategy. Compared with liposomes, cubosomes allow higher loading of hydrophobic drugs [36]. Characterization and evaluation of cubosomes can be conducted using electron microscopy, X-ray scattering, particle size distribution analysis, and entrapment efficiency measurements [37].

The nanoscale dimensions of cubosomes enhance drug penetration and retention within cancerous tissues [37], positioning them as highly effective vehicles for targeted delivery—a fundamental requirement in oncological therapy. Furthermore, cubosomes outperform liposomes because they can accommodate greater internal volumes, enabling the incorporation of larger drug amounts. This results in improved loading capacity and reduced viscosity [38, 39]. Moreover, cubosomes can encapsulate water-soluble drugs within their bilayers. Upon encountering intestinal lipases, these loaded cubosomes break apart into smaller bioadhesive fragments that maintain extended contact with the intestinal lining, thereby facilitating drug uptake and bioavailability [40].

These cubosomes constitute adaptable carrier systems with promising theranostic potential. They can be engineered for delivery via oral, topical, or intravenous routes. Contemporary research has further advanced preparation techniques, therapeutic performance, analytical evaluation, target identification, controlled drug release, and the tailoring of loaded anticancer agents [28]. Cubosome-based delivery has been demonstrated to be effective for compounds such as 5-Fluorouracil, Cisplatin, paclitaxel, Temozolomide, Doxorubicin, and Icarin across a variety of cancer cell types [41].

In the work reported here, NITRO is being investigated for repurposing against breast cancer cells that are known to express the nitroreductases required for its activation. The aim was to formulate NITRO as Cubosomes to leverage their distinctive delivery characteristics and thereby guarantee the agent's therapeutic efficacy.

Materials and Methods

Materials

Nitrofurantoin (NITRO) (a generous gift from Sinochem Jiangsu, China). Poloxamer 407 (PX407) (Fisher Scientific, UK), Glyceryl mono oleate (GMO) at 90–95% purity, and dimethyl formamide (DMF) (Sigma Aldrich, USA). Every other chemical employed was of analytical reagent grade.

Methods

Preparation of NITRO-cubosomes (NITRO-Cs) systems

The lipid-based (oily) phase ingredients of the cubosomes, represented by Poloxamer (PX 407) and Glyceryl monooleate (GMO), were weighed out according to the pre-specified proportions. They were then liquefied in a heated water bath maintained at 60 °C until a homogeneous blend was obtained. The liquefied oily mixture was thoroughly stirred just before the addition of the precisely weighed, matching portion of NITRO. Following this, the oily mixture underwent 10 minutes of high-speed homogenization (High-speed homogenizer, Heidolph Diax 900, Germany) at 10,000 rpm, during which preheated distilled water (60 °C) was dispensed dropwise. This step was followed by a 2-minute treatment with ultrasonic sound waves (Probe Sonicator, GE 130, China), delivered as pulses spaced 2 seconds apart to fragment any clumps that might have formed within the dispersion. Afterward, the systems were allowed to cool and stored in amber-tinted glass vials for 48 hours before any further testing [42].

Full factorial design

The experimental framework was constructed around a 2^3 full-factorial arrangement using the Design-Expert VR software suite (V.7.0.0, Stat-Ease Inc., Minneapolis, USA)—the investigation aimed to determine the influence of three independent variables on specific outcomes. The factors (independent variables) explored were the drug: oil phase ratio (X1), the oil: aqueous phase ratio (X2), and the GMO: PX 407 ratio (X3). The measured outcomes were the Particle Size (PS) of the resulting cubosomes (R1), the Zeta potential (ZP) reading (R2), the Polydispersity Index (PDI) (R3), and the Percentage entrapment efficiency (%EE) (R4). Optimization aimed to achieve the smallest possible PS and PDI while simultaneously maximizing ZP and %EE to pinpoint the system with the greatest desirability. The factors, their corresponding levels, and the limitations applied during the preparation and optimization of NITRO-Cs are outlined in **Table 1**.

Table 1. 23-Factorial design independent variables, their levels, responses, and constraints for NITRO-Cs systems

Independent variables (Factors)	Lower limit	Upper limit
Drug to oily phase ratio (X1)	1:10	2:10
Oily to aqueous phase ratio (X2)	1:10	1:5
GMO to PX 407 ratio (X3)	0.25:1	0.5:1
Responses	**Target/Constraint**	
R1: Particle size (PS)	Minimize	
R2: Zeta potential (ZP)	Maximize	
R3: Polydispersity index (PDI)	Minimize	
R4: Entrapment efficiency (%EE)	Maximize	

Table 1: 2^3-Factorial design independent variables, their levels, responses, and constraints for NITRO-Cs systems.

Characterization of NITRO-cubosomes (NITRO-Cs)

Entrapment Efficiency Percentage (%EE)

The %EE was quantified using the established indirect technique [43]. The NITRO-Cs systems were centrifuged to partition the unentrapped drug into the external medium (Cooling Centrifuge, Centurion Scientific K3 Series, Germany) [44]. Specimens of 2 mL each were transferred to Eppendorf tubes and spun at 14,000 rpm at 4 °C for 10 minutes. The elevated speed, combined with the low temperature, induced solidification and settling of the cubosomes, thereby isolating the aqueous phase that harbors the free, unentrapped drug. A 1 mL aliquot of the clear supernatant was suitably diluted to a final volume of 25 mL with distilled water, after which its UV absorbance was measured at a λ max of 375 nm (UV spectrophotometer (Lab India UV-320, Mumbai, India) [45]. The associated concentration of free NITRO in the supernatant was subsequently deduced from a calibration plot of Nitrofurantoin in distilled water prepared beforehand. Six replicate measurements were conducted for each system. The proportion of entrapped NITRO was computed using the equation presented below:

$$\%EE = \frac{C_{total} - C_{free}}{C_{total}} \times 100 \quad (1)$$

Where C_{free} stands for the calculated amount of free NITRO, and C_{total} indicates the total amount of NITRO available in one mL of the cubosome dispersion.

Particle size (PS), zeta potential (ZP), and polydispersity index (PDI)

The average PS and PDI of the cubosomes, as well as the ZP of the NITRO-Cs systems, were assessed through the laser diffraction principle using a Zeta sizer instrument (Malvern, Nano Series ZS90, Malvern Instruments, Ltd., Worcestershire, UK). A sample portion (0.5 mL) was diluted with 30 mL of distilled water to achieve the desired scattering intensity. All measurements were carried out at 25 °C [46, 47].

In-vitro release study

The release behavior of the system that achieved the highest desirability was profiled. A dialysis membrane (Dialysis Tubing Cellulose Membrane, molecular weight cut-off 12,000–14,000, SERVA GmbH, Heidelberg, Germany) was used to evaluate both the chosen cubosome formulation and the unformulated drug [48]. A 1 mL volume of the selected system (17 mg/mL) or a matching mass of free drug suspended in 1 mL of saline phosphate buffer (PBS), pH 7.4, was introduced into a tube open at one extremity and closed at the other, with the dialysis membrane. This tube was then immersed in 50 mL of PBS (pH 7.4), thermostated at 37 ± 0.5 °C, and stirred at 150 rpm. Samples of 3 milliliters each were retrieved at predetermined intervals—0.5, 1, 2, 3, 4, 5, 6, and 12 hours—with each withdrawal immediately replenished with an identical volume of fresh, warmed buffer. The retrieved samples were suitably diluted using the buffered medium, and the drug was analyzed spectrophotometrically at a λ max of 375 nm. The entire procedure was replicated six times (for each sampling point). The cumulative percentage of drug released was calculated by dividing the amount released at each time point by the initial amount of drug loaded into the dialysis bag. The release data for free NITRO and the optimized formulation were compared at 4 and 8 hours. Statistical analysis of the findings was performed using a Student's T-test.

Transmission electron microscope (TEM)

Transmission electron microscopy (TEM; JEOL JEM-1400, Japan) was used to obtain micrographs of the optimized NITRO-Cs system for morphological assessment. A single droplet of the optimized NITRO-Cs dispersion was diluted with deionized water, applied to a carbon-coated copper grid, and counterstained with a 1% sodium phosphotungstate solution. The grid was set aside to air-dry at ambient temperature before inspection at 200 kV [49].

Cell viability examinations using MCF-7 Cells

The cytotoxic activity of the optimal NITRO-Cs system was assessed against MCF-7 breast cancer cells (Human Breast Cancer Cell Line, VACSERA, Egypt, subcultured from ATCC ® HTB-22™) using an MTT reduction assay [50]. A 96-well tissue culture plate (Microtiter™) was inoculated with 1×10^5 cells/mL and incubated at 37°C for 24 hours to promote cell growth and the formation of an intact cell monolayer. The wells contained the

propagation medium required for cellular multiplication: RPMI-1640 medium fortified with 1% l-glutamine, 10% heat-inactivated fetal bovine serum, 50 µg/mL gentamicin, and HEPES buffer. The chosen NITRO-Cs system was measured against the unformulated drug and the empty cubosomes (drug-free Cubosomes). Test samples were diluted in serial steps (31.25–62.5–125–250–500–1000 µg/mL) using maintenance medium (RPMI medium supplemented with 2% serum), and 0.1 mL of each dilution was dispensed into designated wells (five replicates at each dilution step). These dilutions were contrasted with a control set (2 replicates). The plate was subsequently incubated at 37°C before being scrutinized. Cells were checked for morphological hallmarks of toxicity, including rounding up, partial or complete monolayer detachment, granulation, or cell shrinkage. Thereafter, 20 microliters of MTT solution at a strength of 5 mg/mL in PBS (BIO BASIC CANADA INC) were added to every well and homogenized by agitating the plate on a shaker set to 150 rpm for 5 minutes. The plates were then returned to the incubator (37 °C, 5% CO_2) for 4 hours to allow MTT to be metabolized. The resultant formazan (the metabolic derivative of MTT) was resolubilized in DMSO (200 µL) and blended vigorously. Optical density was measured at 560 nm, with background correction at 620 nm, using a BioTek ELX800 microplate reader. The optical density readings correlated directly with the viable cell count.

Statistical analysis

Design-Expert VR software (V.7.0.0, Stat-Ease Inc., Minneapolis, USA) and Microsoft Excel 2019 were used to execute the full factorial design. Means were contrasted using a factorial ANOVA with a significance cut-off of $p < 0.05$, with a Tukey post hoc test applied subsequently. Numerical optimization [51] was performed following the restrictions listed in **Table 2**. All experiments were run in sextuplicate, and the data were presented as mean ± SD.

Table 2. Composition and results of characterization of NITRO-Cs systems.

S	GMO: PX407 ratio (X3)	Oily: Aqueous phase ratio (X2)	Drug: Oily phase ratio (X1)	%EE (R4)	PDI (R3)	ZP (mV) (R2)	PS (nm) (R1)
1	0.25:1	1:10	2:10	98.7 ± 1.9	0.6 ± 0.0	−19.4 ± 2.8	89.9 ± 1.7
2	0.25:1	1:5	1:10	98.6 ± 1.8	0.3 ± 0.0	−15.9 ± 0.1	34.5 ± 0.1
3	0.25:1	1:10	1:10	97.4 ± 1.0	0.5 ± 0.1	−16.1 ± 0.4	50.5 ± 1.6
4	0.5:1	1:10	1:10	98.0 ± 1.4	0.4 ± 0.0	−7.9 ± 2.2	72.9 ± 0.1
5	0.5:1	1:10	2:10	98.3 ± 1.6	0.4 ± 0.1	−8.2 ± 0.8	57.7 ± 0.4
6	0.5:1	1:5	1:10	98.6 ± 1.8	0.3 ± 0.0	−13.4 ± 0.6	45.5 ± 1.1
7	0.5:1	1:5	2:10	98.1 ± 1.4	0.4 ± 0.0	−23.8 ± 1.4	50.9 ± 3.9
8	0.25:1	1:5	2:10	97.9 ± 1.3	0.6 ± 0.1	−8.6 ± 0.7	52.9 ± 2.1

Results and Discussion

All fabricated NITRO-C systems yielded homogeneous, milky-yellow suspensions that exhibited no signs of aggregation. In accordance with the experimental layout, eight NITRO-loaded systems were assessed; their compositional breakdown and characterization results are presented in **Table 2**.

Table 2 Composition and results of characterization of NITRO-Cs systems.

All three factors—drug: oily phase ratio, oily: aqueous phase ratio, and GMO: PX407 ratio—had a notable effect on PS ($P = 0.0006$). Smaller PS values were favored by a low drug: oil phase ratio, a high oil: aqueous phase ratio, and a high GMO: PX407 ratio.

ZP was appreciably influenced by the factors examined ($P = 0.0141$). A rise in ZP followed an upturn in the drug: oil phase ratio, the oily: aqueous phase ratio, and the GMO: PX407 ratio.

The dispersion's size distribution, as indicated by PDI, was substantially influenced by the explored factors ($P < 0.0001$). Reduced PDI values were associated with a low drug: oil phase ratio, a high oil: aqueous phase ratio, and a high GMO: PX407 ratio.

Figure 1 portrays the interplay among the factors under study and their respective influences on PS, ZP, and PDI.

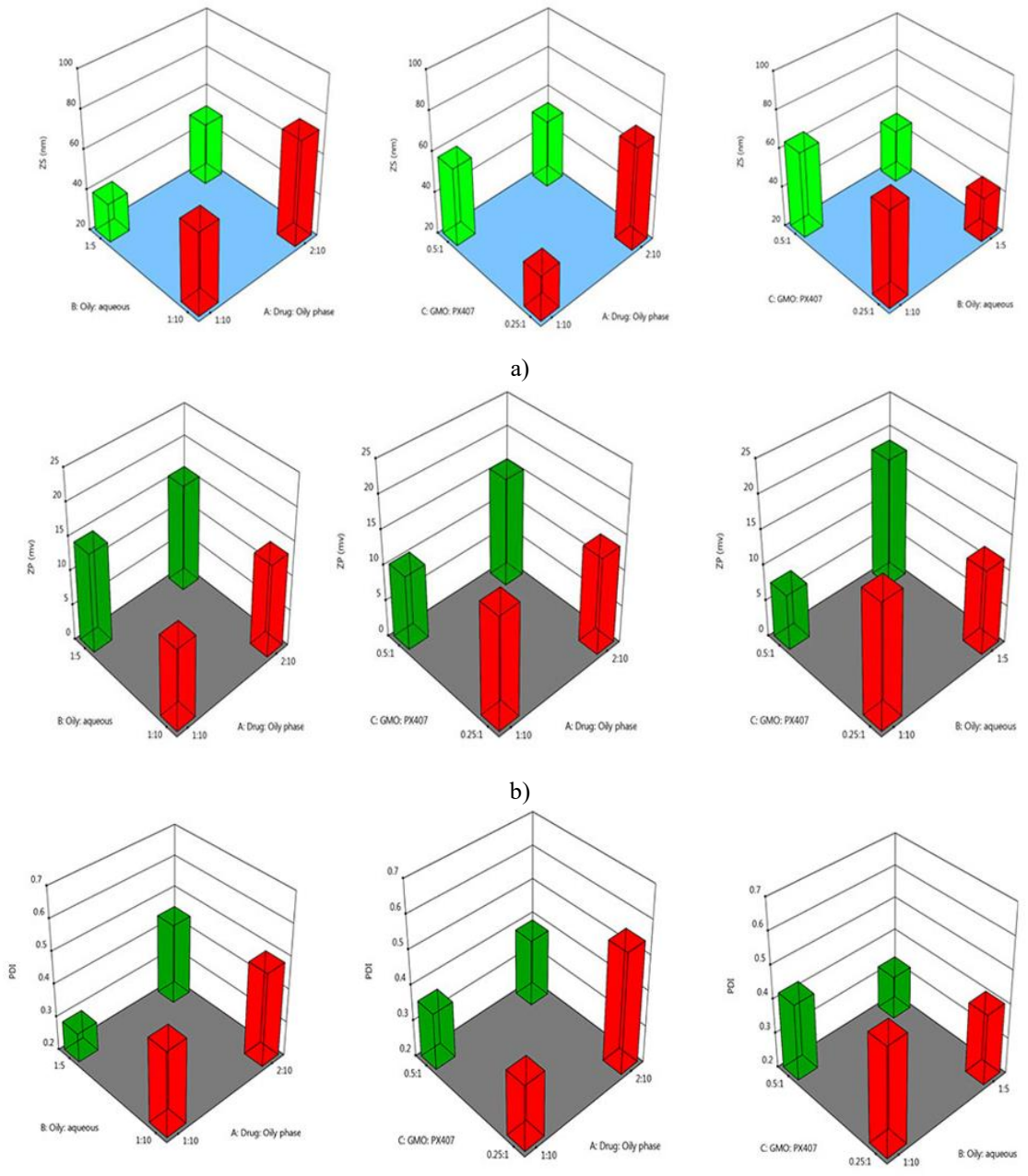

a)

b)

c)

Figure 1. Effects of interactions between the studied factors on Nitrofurantoin cubosome system PS (a), ZP (b), and PDI (c).

A desirability strategy, based on the analysis of factorial design outputs, was employed to achieve numerical optimization. The procedure was carried out to pinpoint the X1, X2, and X3 levels that would keep system PS and PDI to a minimum while pushing ZP and %EE to a maximum. Desirability ratings extended from 0 to 1. The optimized system was S6, which had the highest desirability score (0.774). Its makeup was a 1:10 Drug: Oily phase ratio, a 1:5 Oily: Aqueous phase ratio, and a 0.5:1 GMO:PX407 ratio.

In view of this, system S6 was earmarked for deeper scrutiny, during which its release behavior was mapped. **Figure 2** depicts the release pattern of NITRO from the S6 system side by side with the free drug.

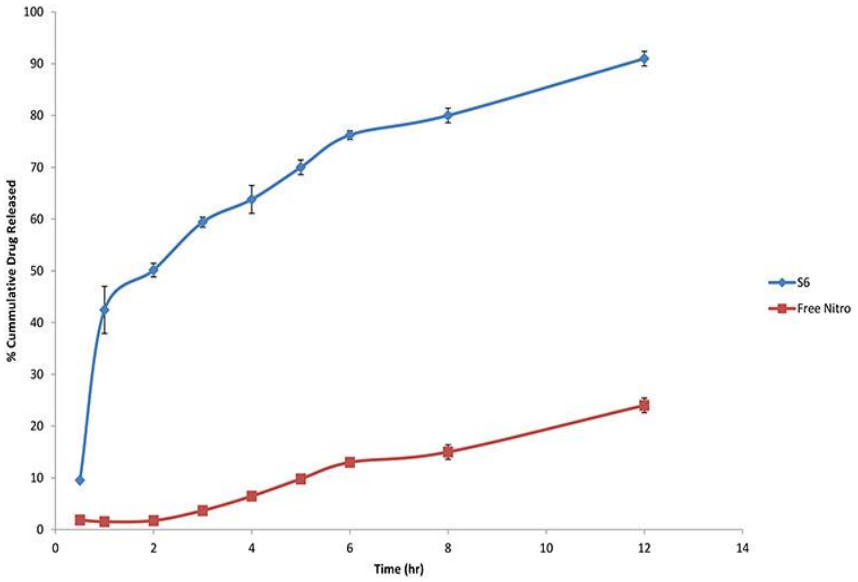

Figure 2. Cumulative Percentage of drug released from S6 Vs Free NITRO.

Figure 2 shows the markedly better drug release performance of S6 compared with free NITRO at 4 hours ($P = 0.00055$) and 8 hours ($P = 0.000237$).

Kinetic fitting of drug liberation from S6 uncovered zero-order release kinetics ($R^2 = 0.8929$ for zero order, $R^2 = 0.4689$ for first order, $R^2 = 0.889$ for the Higuchi model).

TEM imaging of S6 **(Figure 3)** revealed cubosome architectures spanning spherical to polygonal outlines. A recognizable dark-stained external shell and a markedly paler interior, housing the entrapped drug, were clearly distinguishable. The particle dimensions appeared to lie beneath 50 nm.

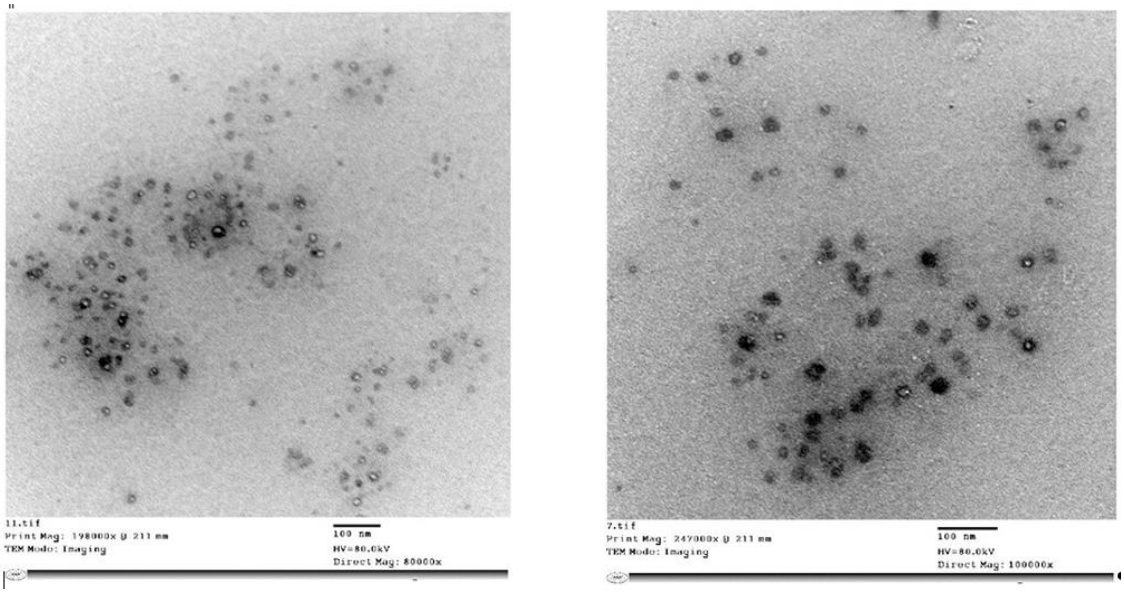

a) b)

Figure 3. TEM photographs of S6.

S6 was evaluated for cytotoxicity against MCF-7 breast cancer cells. A series of dilutions of S6, free NITRO, and drug-free cubosomes were probed for their cytotoxic action. **Figure 4** shows the percentage cell survival for S6, free NITRO, and the drug-free cubosomes at the tested dilutions.

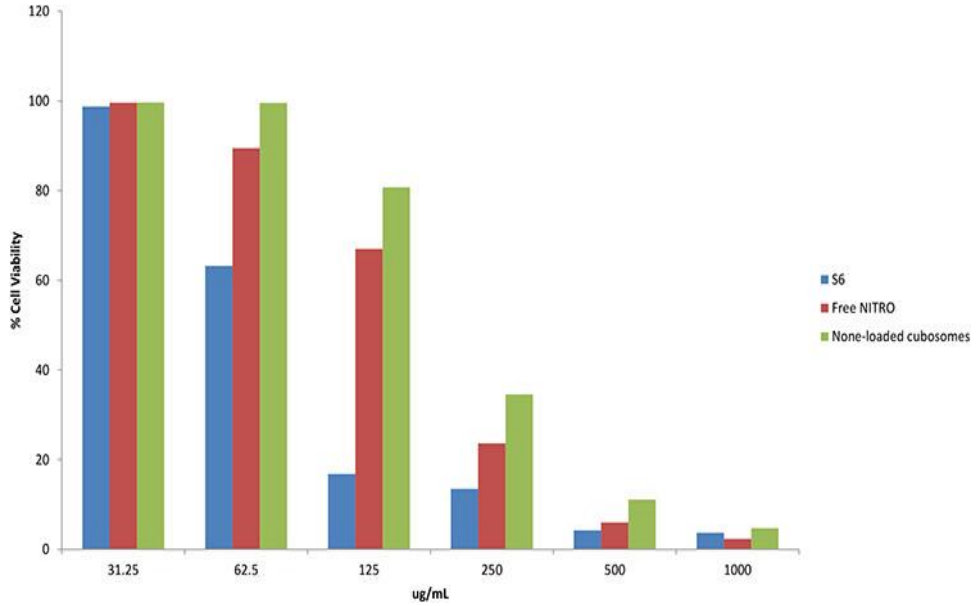

Figure 4. Effects of different dilutions of S6, Free NITRO, and None-loaded Cubosomes on MCF-7 cells.

Figure 4 exposed a more pronounced cytotoxic action of S6 relative to both free NITRO and the drug-free cubosomes. Derivation of IC50 values underscored the potency of S6 at diminished concentrations, as illustrated in **Figure 5.**

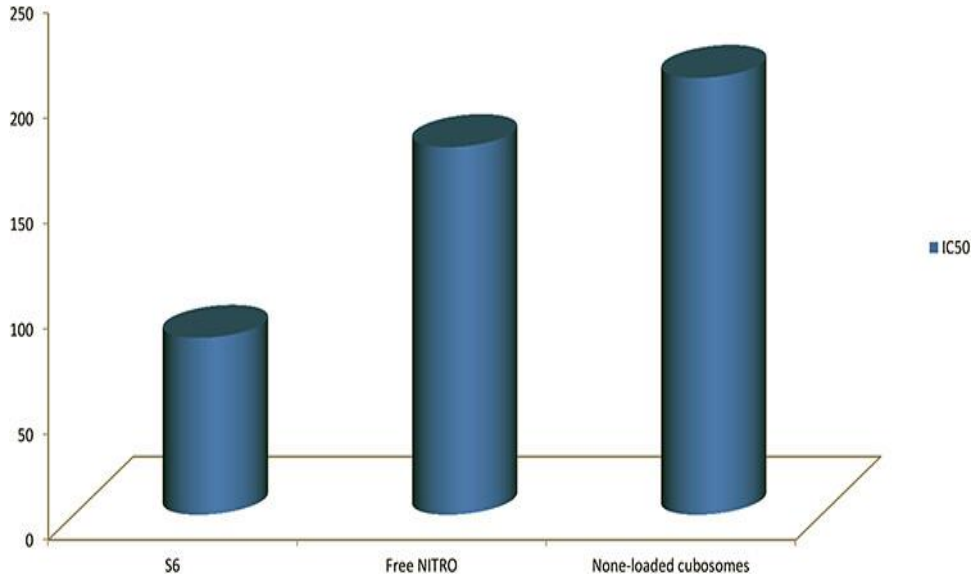

Figure 5. IC50 for S6 compared to free nitro and non-loaded cubosomes.

ANOVA comparison of the IC50 estimates established that S6 possessed a meaningfully reduced value (83.99 ± 0.15 µg g/mL) in contrast to Free NITRO (174.54 ± 1.36 µg g/mL) and Drug-free Cubosomes (207.38 ± 0.59 µg g/mL) (P = 0.000).

The impact of S6, free NITRO, and Drug-free Cubosomes on cell viability was reflected in cells morphology when compared with the control cell cohort. Hallmarks of cellular distress were apparent in **Figure 6**, manifested by the appearance of shrunken, rounded cells.

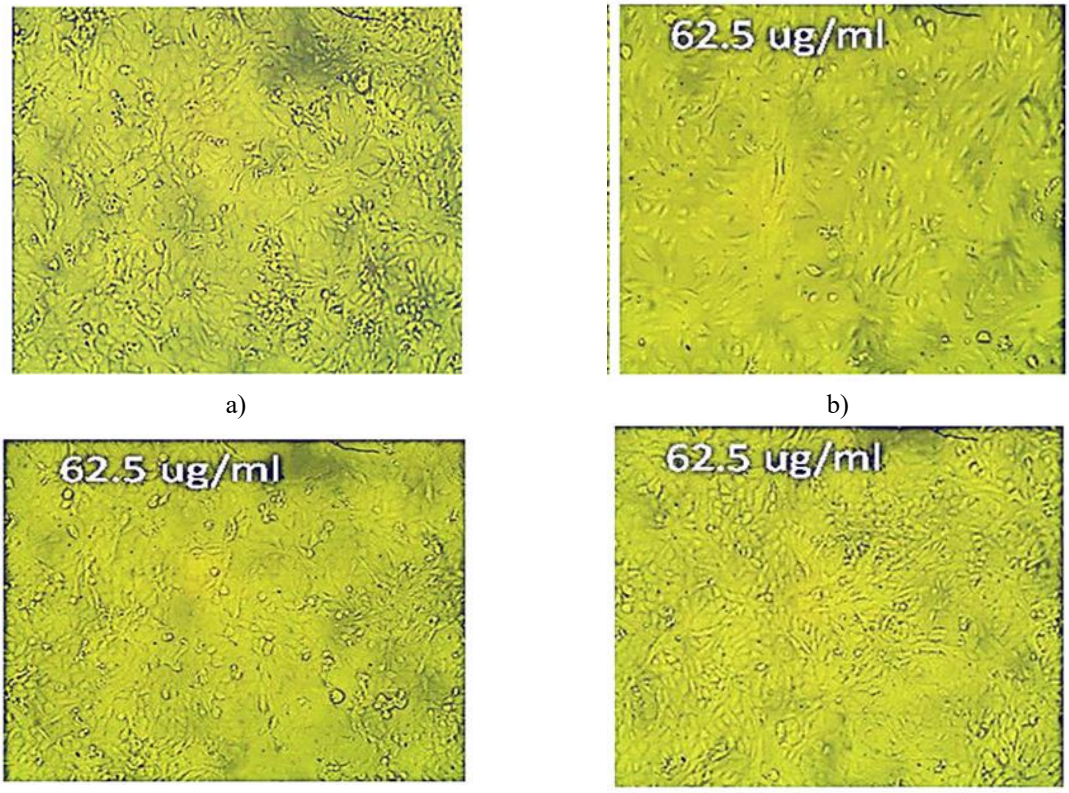

a) b)

c) d)

Figure 6. Inverted microscope photos of (a) Control MCF-7 cells; (b) 62.5 ug/mL of S6; (c) Free NITRO and (d) None-loaded Cubosomes.

Drawing on the outcomes compiled in **Table 2**, all NITRO-Cs systems displayed elevated %EE values, ranging from 97.43% to 98.71%. ANOVA of the data indicated that superior entrapment efficiency was associated with a high oily:aqueous phase ratio and a high GMO:PX407 ratio ($P = 0.0007$). This arose from the inherently low aqueous solubility of the drug, which drove its sequestration within the oily bilayer among the alkyl chains that constitute the GMO framework, independently of the quantity of GMO present relative to the drug load or water volume [52, 53].

An upturn in PS paralleled an increase in the drug fraction, corroborating earlier reports linking larger particle size to higher drug payloads in Flurbiprofen cubosome formulations [54]. Whilst higher proportions of PX407 (equating to a low GMO: PX407 ratio) were conducive to smaller PS, these proportions could simultaneously induce the formation of alternative vesicular configurations coexisting with cubosomes [55]. This accounted for the observation of a comparatively broad size distribution (PDI) at a low GMO: PX407 ratio.

The formulated systems displayed negative ZP values, a trait attributable to the negatively charged free oleic acid residues on the GMO backbone [56]. A higher ZP magnitude was observed with the elevated lipid fraction delivered by a higher GMO proportion (high GMO: PX407 ratio), consistent with published findings showing that Resveratrol cubosomes formulated with the maximal GMO proportion exhibited the highest ZP magnitude [57].

The optimal system, identified through desirability computation, was S6 and was subsequently taken forward for further exploration encompassing drug release kinetics, TEM visualization, and cytotoxicity evaluation.

The release behavior of free NITRO versus S6 is shown in **Figure 2**, which demonstrates a statistically significant advantage in the percentage of drug released from S6 over free NITRO after 4 hours ($P = 0.00055$) and 8 hours ($P = 0.000237$). This was ascribed to the solubilizing capability of PX407, which enabled NITRO to be released from the cubosomes into the dissolution medium [58]. The figure further indicated that S6 exhibited two discrete drug liberation rates: an initial stage characterized by a more rapid release tempo, followed by a slower tempo. This phenomenon could be rationalized by the presence of drug molecules initially dissolved within the oily architecture, providing a vast surface area (nanoscale dimensions) for exposure to the dissolution medium. Subsequently, a decelerated release profile emerged as drug diffusion from the labyrinthine internal geometry of

the cubosomes into the dissolution medium became the rate-limiting step. These observations aligned with earlier literature describing a biphasic liberation profile for Clopidogrel Bisulfate cubosomes, a pattern attributed to the considerable surface area inherent to nanoparticulate systems [27]. The adherence of S6 to zero-order release kinetics secured a uniform rate of drug delivery spanning an extended period [59].

The outcomes of the MCF-7 cell-based experiments confirmed that NITRO can enter cells and induce stress and cytotoxicity, whether delivered in its free form or packaged in cubosomes. The well-documented mode of action of NITRO, rooted in its history as an established antibacterial, hinges on its conversion into strongly electrophilic reactive intermediates by Nitro reductases. These intermediates attach to ribosomal proteins, blocking protein manufacture and ultimately causing cellular damage [20]. Reports have shown that breast cancer cells exhibit overexpression of the Nitroreductase enzyme [60]. This knowledge indicates that NITRO, when situated in proximity to breast cancer cells, undergoes activation via the expression of Nitro reductase, leading to suppression of protein synthesis by NITRO. As a result, NITRO induced cytotoxicity in MCF-7 cells, both as Free NITRO and in the S6 (cubosomal formulation). The marked advantage of S6 over free NITRO, underscored by a substantially reduced IC50 (83.99 ± 0.15 µg g/mL) relative to free NITRO (174.54 ± 1.36 µg g/mL), can be explained by the entrapment of NITRO within the cubosome architecture. The minute size of cubosomes, together with their capacity to adapt to membrane curvature, facilitated better drug retention and improved permeation into cells [28, 31].

The cytotoxic effect observed with the unloaded cubosomes was marginal, as reflected by a substantially higher IC50 (207.38 ± 0.59 µg g/mL) [61]. Paradoxically, these elevated concentration thresholds verified the biocompatibility of unloaded cubosomes with normal cells when dosing is performed at the effective S6 level.

Conclusion

Accordingly, the decades-old antibiotic NITRO, which has been used effectively to treat urinary tract infections, can once again become a focus of research through repurposing. NITRO, classified in Class IV of the biopharmaceutical system, can achieve improved solubility and enhanced cellular internalization through cubosomal entrapment. NITRO Cubosomes were engineered via hot homogenization in accordance with a 2^3 full-factorial design. S6 (comprising a 1:10 drug: oily phase ratio, a 1:5 oily: aqueous phase ratio, and a 0.5:1 GMO: PX407 ratio) demonstrated the greatest desirability and was chosen for subsequent examination. In a cubosomal delivery platform (S6), NITRO produced cytotoxic effects against breast cancer cells, a phenomenon driven by its bioactivation via the Nitro reductase enzyme shed by the malignant cells and by the superior permeability afforded by the cubosomal shell, while safeguarding normal cells. Thus, NITRO, by resurging in breast cancer management, can contribute to achieving one of the aims of sustainable development. It is therefore recommended to proceed with further in vivo and stability investigations.

Acknowledgments: None

Conflict of Interest: None

Financial Support: None

Ethics Statement: None

References

1. Mansoori B, Mohammadi A, Davudian S, Shirjang S, Baradaran B. The different mechanisms of cancer drug resistance: a brief review. Adv Pharm Bull. 2017;7(3):339-48. doi:10.15171/apb.2017.041
2. Anand U, Dey A, Chandel AKS, Sanyal R, Mishra A, Pandey DK, et al. Cancer chemotherapy and beyond: current status, drug candidates, associated risks and progress in targeted therapeutics. Genes Dis. 2023;10(4):1367-400. doi:10.1016/j.gendis.2022.02.007
3. Debela DT, Muzazu SGY, Heraro KD, Ndalama MT, Mesele BW, Haile DC, et al. New approaches and procedures for cancer treatment: current perspectives. SAGE Open Med. 2021;9:20503121211034366. doi:10.1177/20503121211034366

4. Chupradit S, Widjaja G, Majeed BR, Jalil AT, Abdelbasset WK, Yumashev AV, et al. Recent advances in cold atmospheric plasma (CAP) for breast cancer therapy. Cell Biol Int. 2023;47(2):327-40.
5. Moura C, Correia AS, Pereira M, Ribeiro E, Santos J, Vale N. Atorvastatin and nitrofurantoin repurposed in the context of breast cancer and neuroblastoma cells. Biomedicines. 2023;11(3):903-23.
6. Rabelo ACS, Guerreiro CA, Shinzato VI, Ong TP, Noratto G. Anthocyanins reduce cell invasion and migration through Akt/mTOR downregulation and apoptosis activation in triple-negative breast cancer cells: a systematic review and meta-analysis. Cancers (Basel). 2023;15(18):2300-13.
7. El-Tanani M, Platt-Higgins A, Lee Y, Pawade J, Morgan L, Rytina E, et al. Matrix metalloproteinase 2 is a target of the RAN-GTP pathway and mediates migration, invasion and metastasis in human breast cancer. Life Sci. 2022;310:121086.
8. Guo Z, Zhang H, Fu Y, Wang H, Li Y, Xu J, et al. Cancer-associated fibroblasts induce growth and radioresistance of breast cancer cells through paracrine IL-6. Cell Death Discov. 2023;9:1-10.
9. Hernandes EP, Lazarin-Bidóia D, Bini RD, Nakamura CV, Cótica LF, de Oliveira Silva Lautenschlager S. Doxorubicin-loaded iron oxide nanoparticles induce oxidative stress and cell cycle arrest in breast cancer cells. Antioxidants (Basel). 2023;12(2):273-89.
10. Ashrafizadeh M, Zarrabi A, Bigham A, Samadi M, Najafi M, Farhood B, et al. (Nano)platforms in breast cancer therapy: drug/gene delivery, advanced nanocarriers and immunotherapy. Med Res Rev. 2023;43(2):1-15.
11. Yang F, He Q, Dai X, Zhang X, Song D. The potential role of nanomedicine in the treatment of breast cancer to overcome the obstacles of current therapies. Front Pharmacol. 2023;14:1-12.
12. Dongsar TT, Dongsar TS, Abourehab MA, Gupta N, Kesharwani P. Emerging application of magnetic nanoparticles for breast cancer therapy. Eur Polym J. 2023;187:111881.
13. Rajaei M, Rashedi H, Yazdian F, Navaei-Nigjeh M, Rahdar A, Díez-Pascual AM. Chitosan/agarose/graphene oxide nanohydrogel as drug delivery system of 5-fluorouracil in breast cancer therapy. J Drug Deliv Sci Technol. 2023;82:104350.
14. Xu J, Lai Y, Wang F, Zhang Y, Liu X, Chen H, et al. Dual stimuli-activatable versatile nanoplatform for photodynamic therapy and chemotherapy of triple-negative breast cancer. Chin Chem Lett. 2023;34(12):108800.
15. Taha S, Mohamed WR, Elhemely MA, El-Gendy AO, Mohamed T. Tunable femtosecond laser suppresses the proliferation of breast cancer in vitro. J Photochem Photobiol B. 2023;240:112658.
16. Sleire L, Førde HE, Netland IA, Leiss L, Skeie BS, Enger PØ. Drug repurposing in cancer. Pharmacol Res. 2017;124:74-91.
17. Crofts TS, Sontha P, King AO, Wang B, Biddy BA, Zanolli N, et al. Discovery and characterization of a nitroreductase capable of conferring bacterial resistance to chloramphenicol. Cell Chem Biol. 2019;26(4):559-70.
18. Andrade JK, Souza MI, Gomes Filho MA, Figueiredo KA, Oliveira JS, Nunes XP, et al. N-pentyl-nitrofurantoin induces apoptosis in HL-60 leukemia cell line by upregulating BAX and downregulating BCL-xL gene expression. Pharmacol Rep. 2016;68(5):1046-53.
19. Race PR, Lovering AL, Green RM, Ossor A, White SA, Searle PF, et al. Structural and mechanistic studies of Escherichia coli nitroreductase with the antibiotic nitrofurazone: reversed binding orientations in different redox states of the enzyme. J Biol Chem. 2005;280(14):13256-64.
20. Wang Y, Gray JP, Mishin V, Heck DE, Laskin DL, Laskin JD. Role of cytochrome P450 reductase in nitrofurantoin-induced redox cycling and cytotoxicity. Free Radic Biol Med. 2008;44(6):1169-79.
21. Al-Masoudi NA, Al-Soud YA, Kalogerakis A, Pannecouque C, De Clercq E. Nitroimidazoles, part 2: synthesis, antiviral and antitumor activity of new 4-nitroimidazoles. Chem Biodivers. 2006;3(5):515-26.
22. Chen Z, Han F, Du Y, Shi H, Zhou W. Hypoxic microenvironment in cancer: molecular mechanisms and therapeutic interventions. Signal Transduct Target Ther. 2023;8(1):70.
23. Manin AN, Voronin AP, Boycov DE, Drozd KV, Churakov AV, Perlovich GL. A combination of virtual and experimental screening tools for the prediction of nitrofurantoin multicomponent crystals with pyridine derivatives. Crystals (Basel). 2023;13(7):1022.
24. Dadwal A, Baldi A, Kumar Narang R. Nanoparticles as carriers for drug delivery in cancer. Artif Cells Nanomed Biotechnol. 2018;46(1):295-305.

25. Yao Y, Zhou Y, Liu L, Xu Y, Chen Q, Wang Y, et al. Nanoparticle-based drug delivery in cancer therapy and its role in overcoming drug resistance. Front Mol Biosci. 2020;7:193.
26. Khan R, Arshad A, Hassan IU, Aslam MS, Khan MR, Bibi S, et al. Advances in nanomaterial-based immunosensors for prostate cancer screening. Biomed Pharmacother. 2022;155:113690.
27. El-Laithy H, Badawi A, Abdelmalak NS, El-Sayyad N. Cubosomes as oral drug delivery systems: a promising approach for enhancing the release of clopidogrel bisulphate in the intestine. Chem Pharm Bull (Tokyo). 2018;66(12):1165-73.
28. Varghese R, Salvi S, Sood P, Kulkarni B, Kumar D. Cubosomes in cancer drug delivery: a review. Colloids Interface Sci Commun. 2022;46:100570.
29. Garg G, Saraf S, Saraf S. Cubosomes: an overview. Biol Pharm Bull. 2007;30(2):350-3.
30. Shetty S, Shetty S. Cubosome-based cosmeceuticals: a breakthrough in skincare. Drug Discov Today. 2023;28(7):103623.
31. Zhang L, Li J, Tian D, Sun L, Wang X, Tian M. Theranostic combinatorial drug-loaded coated cubosomes for enhanced targeting and efficacy against cancer cells. Cell Death Dis. 2020;11(1):1.
32. Murgia S, Falchi AM, Mano M, Lampis S, Angius R, Carnerup AM, et al. Nanoparticles from lipid-based liquid crystals: emulsifier influence on morphology and cytotoxicity. J Phys Chem B. 2010;114(10):3518-25.
33. Yaghmur A, Glatter O. Characterization and potential applications of nanostructured aqueous dispersions. Adv Colloid Interface Sci. 2009;147-148:333-42.
34. Janakiraman K, Krishnaswami V, Sethuraman V, Rajendran V, Kandasamy R. Development of methotrexate-loaded cubosomes with improved skin permeation for the topical treatment of rheumatoid arthritis. Appl Nanosci. 2019;9(8):1781-96.
35. Madheswaran T, Kandasamy M, Bose R, Karuppagounder V. Current potential and challenges in the advances of liquid crystalline nanoparticles as drug delivery systems. Drug Discov Today. 2019;24(7):1405-12.
36. Leibrock L, Wagener S, Singh AV, Laux P, Luch A. Nanoparticle induced barrier function assessment at liquid-liquid and air-liquid interface in novel human lung epithelia cell lines. Toxicol Res (Camb). 2019;8(6):1016-27.
37. Sivadasan D, Sultan MH, Alqahtani SS, Javed S, Afzal O, Alanazi FG, et al. Cubosomes in drug delivery—a comprehensive review on its structural components, preparation techniques and therapeutic applications. Biomedicines. 2023;11(4):1114.
38. Siekmann B, Bunjes H, Koch MHJ, Westesen K. Preparation and structural investigations of colloidal dispersions prepared from cubic monoglyceride-water phases. Int J Pharm. 2002;244(1-2):33-43.
39. Meli V, Caltagirone C, Falchi AM, Murgia S, Sgarrella F, Manconi M, et al. Docetaxel-loaded fluorescent liquid-crystalline nanoparticles for cancer theranostics. Langmuir. 2015;31(35):9566-75.
40. Salem EM, Dawaba H, Gad S, Hassan TH. Cubosomes as an oral drug delivery system. Rec Pharm Biomed Sci. 2023;7(3):81-90.
41. Umar HA, Wahab H, Gazzali AM, Tahir H, Ahmed W. Cubosomes: design, development, and tumor-targeted drug delivery applications. Polymers (Basel). 2022;14(15):3118.
42. El-Hashemy HA, Salama A, Rashad A. Experimental design, formulation, and in vivo evaluation of novel anticoagulant rivaroxaban-loaded cubosomes in rats model. J Liposome Res. 2022;32(4):1-8.
43. Zewail M, Gaafar PME, Ali MM, Abbasa H. Lipidic cubic-phase leflunomide nanoparticles (cubosomes) as a potential tool for breast cancer management. Drug Deliv. 2022;29(1):1663-74.
44. Nasr M, Younes H, Abdel-Rashid RS. Formulation and evaluation of cubosomes containing colchicine for transdermal delivery. Drug Deliv Transl Res. 2020;10(5):1302-13.
45. Cair MR, Pienaar EW, Lotter AP. Polymorphism and pseudopolymorphism of the antibacterial nitrofurantoin. Mol Cryst Liq Cryst. 1996;279(1):241-64.
46. Marques C, Maurizi L, Borchard G, Jordan O. Characterization challenges of self-assembled polymer-SPION nanoparticles: benefits of orthogonal methods. Int J Mol Sci. 2022;23(1):1-17.
47. Hashem F, Nasr M, Youssif M. Formulation and characterization of cubosomes containing REB for improvement of oral absorption of the drug in human volunteers. J Adv Pharm Res. 2018;2(2):95-103.
48. Elsayad M, Mowafy HA, Zaky AA, Samy AA. Chitosan-caged liposomes for improving oral bioavailability of rivaroxaban: in vitro and in vivo evaluation. Pharm Dev Technol. 2021;26(3):316-27.

49. Chettupalli AK, Ananthula M, Amarachinta PR, Bakshi V, Yata VK. Design, formulation, in vitro and ex vivo evaluation of atazanavir-loaded cubosomal gel. Biointerface Res Appl Chem. 2021;11(4):12037-54.
50. Kamel AA, Fadel M, Louis D. Curcumin-loaded nanostructured lipid carriers prepared using Peceol™ and olive oil in photodynamic therapy: development and application in breast cancer cell line. Int J Nanomedicine. 2019;14:5073-85.
51. Shah M, Pathak K. Development and statistical optimization of solid lipid nanoparticles of simvastatin by using 2^3 full-factorial design. AAPS PharmSciTech. 2010;11(2):489-96.
52. Flak DK, Adamski V, Nowaczyk G, Szutkowski K, Synowitz M, Jurga S, et al. AT101-loaded cubosomes as an alternative for improved glioblastoma therapy. Int J Nanomedicine. 2020;15:7415-31.
53. Segalina A, Pavan B, Ferretti V, Canossa S, Prati F, Benfenati V, et al. Cocrystals of nitrofurantoin: how coformers can modify its solubility and permeability across intestinal cell monolayers. Cryst Growth Des. 2022;22(5):3090-106.
54. Han S, Shen J, Gan Y, Geng H, Zhang X, Zhu C, et al. Novel vehicle based on cubosomes for ophthalmic delivery of flurbiprofen with low irritancy and high bioavailability. Acta Pharmacol Sin. 2010;31(8):990-8.
55. Nasr M, Ghorab MK, Abdelazem A. In vitro and in vivo evaluation of cubosomes containing 5-fluorouracil for liver targeting. Acta Pharm Sin B. 2015;5(1):79-88.
56. Hakim E, El-Mahrouk GM, Abdelbary G, Teaima MH. Freeze-dried clopidogrel-loaded lyotropic liquid crystal: Box-Behnken optimization, in vitro and in vivo evaluation. Curr Drug Deliv. 2020;17(3):207-17.
57. Abdel-Bar HM, Sanad RA. Endocytic pathways of optimized resveratrol cubosomes capturing into human hepatoma cells. Biomed Pharmacother. 2017;93:561-9.
58. Zaki RM, Abou El Ela AE, Almurshedi AS, Aldosari BN, Aldossari AA, Ibrahim MA. Fabrication and assessment of orodispersible tablets loaded with cubosomes for the improved anticancer activity of simvastatin against the MDA-MB-231 breast cancer cell line. Polymers (Basel). 2023;15(7):1774.
59. Adepu S, Ramakrishna S. Controlled drug delivery systems: current status and future directions. Molecules. 2021;26(19):5905.
60. Lu S, Wei L, He W, Zhang X, Wang J, Li Y, et al. Recent advances in the enzyme-activatable organic fluorescent probes for tumor imaging and therapy. ChemistryOpen. 2022;11(10):e202200120.
61. Almoshari Y, Alam MI, Bakkari MA, Alharbi KS, Alzarea SI, Katubi KM, et al. Formulation, characterization, and evaluation of doxorubicin-loaded cubosome as a cytotoxic potentiator against HCT-116 colorectal cancer cells. Indian J Pharm Educ Res. 2022;56(3):723-31.